

Quantum Key Distribution with a Negatively Charged Quantum Dot Single-Photon Source

PARVENDRA KUMAR^{1,*}

¹ Optics and Photonics Centre, Indian Institute of Technology Delhi, Hauz Khas, New Delhi-110016, India
*parvendra@iitd.ac.in

Compiled January 27, 2026

Various quantum key distribution protocols require bright single-photon sources with a very low probability of multiphoton emission. In this work, we investigate single-photon generation from a negatively charged quantum dot embedded in an elliptical pillar microcavity, driven using either resonant excitation or adiabatic rapid passage (ARP). Our results show that ARP excitation significantly suppresses multiphoton emission probability and improves photon indistinguishability compared to resonant excitation. We further evaluate the secure key rate of both BB84 and twin-field quantum key distribution (TF-QKD) using quantum-dot single-photon source and compare its performance with that of Poisson-distributed photon sources (PDS) such as weak coherent pulses and down-conversion sources. The analysis reveals that adiabatic excitation offers a modest but consistent enhancement in secure key rate relative to resonant excitation. Moreover, quantum-dot single-photon sources outperform PDS sources over short and intermediate distances; however, at longer distances, PDS sources eventually surpass quantum-dot sources in both infinite decoy-state BB84 and TF-QKD.

<http://dx.doi.org/10.1364/ao.XX.XXXXXX>

1. INTRODUCTION

The distribution of secret cryptographic keys between the distant parties using the fundamental principles of quantum mechanics is a crucial step for exchanging the information with unconditional security. This process is generally known as quantum key distribution (QKD). Since the first proposal by Charles Bennett and Gilles Brassard in 1984 (BB84), QKD has evolved from a theoretical concept to a full-fledged research area with practical applications [1–6]. The secret keys can be established by appropriately distributing and measuring the quantum bits between two legitimate parties [7–10]. Quantum bits (qubits) can be realized in the different degrees of freedom of single-photon or entangled-photon states. These quantum states are produced via various platforms, including atoms, nonlinear crystals, and semiconductor quantum dots, and can be used to construct QKD methods [11–15]. The quantum principles, like the no-cloning theorem and the disturbance caused by quantum measurements, provide the information-theoretic security since any eavesdropping attempt is reflected as an increase in the quantum bit error rate (QBER). Accordingly, the key distribution protocols can be aborted if the QBER increases beyond a threshold value. Generally, most of the experimental works of QKD employ the weak coherent sources. However, such sources are inherently Poissonian, which means that the weak pulses occasionally contain multiple photons. This situation opens the window for photon-number-splitting (PNS) attacks, which severely restrict both

secure communication distance and key rate [16–20]. However, this problem can be overcome by adding multiple intensity levels—specifically, signal and decoy states—which allow the infinite and realistic decoy-state BB84 protocols and enable Alice and Bob to precisely estimate the single-photon yield and error rate, thereby restoring security that is comparable to that of an ideal single-photon source [21–25].

Another significant development is twin-field quantum key distribution (TF-QKD), which makes it possible to overcome the basic linear rate-distance constraint for point-to-point QKD [26]. TF-QKD allows for much greater operating distances by achieving a key rate that scales with the square root of channel transmittance rather than linearly by interfering weak optical beams from two distant users at an untrusted central station. But TF-QKD's weak coherent states are vulnerable to PNS assaults once more. These vulnerabilities are eliminated by integrating the decoy-state approach with TF-QKD, which offers precise estimation of single-photon contributions. Without using quantum repeaters, secure key distribution over fiber lines longer than 800 km has been made possible via decoy-state TF-QKD and its variations [27–30].

To investigate the performance of quantum key distribution (QKD), we first theoretically analyze single-photon generation from a negatively charged quantum dot driven by resonant excitation and adiabatic rapid passage (ARP). Our results show that ARP excitation enables higher source brightness while sig-

nificantly suppressing multiphoton emission compared to conventional resonant driving. Using these improved source characteristics, we evaluate the secure key rate (SKR) achievable in the BB84 protocol without and with infinite decoy states, as well as in the original twin-field QKD (TF-QKD) protocol with infinite decoy states. We find that the quantum-dot single-photon source outperforms PDS at short and intermediate transmission distances for both BB84 and TF-QKD under the infinite-decoy assumption. Furthermore, the enhanced brightness and reduced multiphoton contribution provided by ARP lead to a consistent additional improvement in the SKR compared to resonant excitation. While previous studies have investigated quantum cryptography using neutral quantum-dot emitters under various excitation schemes [31], the present work focuses instead on an adiabatically driven, negatively charged quantum dot embedded in an elliptical micropillar cavity and operating at telecommunication wavelengths [32, 33]. In addition, embedding the charged quantum dot in an elliptical micropillar cavity relaxes the stringent polarization-filtering requirements typically needed to suppress residual pump light, thereby improving the overall source efficiency [34].

2. THEORY: MODELLING OF SINGLE-PHOTON GENERATION

We consider in-plane excitation of a negatively charged quantum dot (QD) in an elliptical pillar microcavity. The number of distributed Bragg reflectors (DBRs) at the bottom side of the microcavity is assumed to be greater than that on the top side, facilitating photon emission predominantly from the top of the microcavity [34, 35]. The spin states of a single confined electron along the x -axis are represented by $|1\rangle = |\uparrow_x\rangle = \frac{1}{\sqrt{2}}(|\uparrow_z\rangle + |\downarrow_z\rangle)$ and $|2\rangle = |\downarrow_x\rangle = \frac{1}{\sqrt{2}}(|\uparrow_z\rangle - |\downarrow_z\rangle)$. Similarly, the trion states are given by $|3\rangle = |\uparrow_x\downarrow_x\uparrow_x\rangle$ and $|4\rangle = |\uparrow_x\downarrow_x\downarrow_x\rangle$, where \uparrow_x and \downarrow_x represent the heavy-hole spin states along the positive and negative x -axis, respectively. The two ground states $|1\rangle$ and $|2\rangle$ are optically coupled to the excited states $|3\rangle$ and $|4\rangle$ via horizontally (H) and vertically (V) polarized laser fields, as depicted in Fig. 1 (b). Here, ω_0 denotes the energy separation between the ground and excited states in the absence of an externally applied magnetic field. The spin and trion states are energetically split due to the Zeeman energies $\delta_e = g_e\mu_BB$ and $\delta_h = g_h\mu_BB$, respectively. Here, g_e and g_h are the Landé g -factors of the electron and heavy hole, μ_B is the Bohr magneton, and B is the externally applied magnetic field along the x -axis.

The dynamics of the spin states coupled to orthogonally polarized cavity modes and driven by a horizontally polarized laser pulse are described by the Hamiltonian $H = H_0 + H_{\text{int}}$, where H_0 represents the free Hamiltonian of the quantum dot and cavity modes, and H_{int} describes their interaction. These are given by [36] as $H_0 = -\frac{\delta_e}{2}\sigma_{11} + \frac{\delta_e}{2}\sigma_{22} + \left(\omega_0 - \frac{\delta_e}{2}\right)\sigma_{33} + \left(\omega_0 + \frac{\delta_h}{2}\right)\sigma_{44} + \omega_h a^\dagger a + \omega_v b^\dagger b$, and $H_{\text{int}} = g_h a^\dagger (\sigma_{14} + \sigma_{23}) + i g_v b^\dagger (\sigma_{24} + \sigma_{31}) + \Omega_h e^{i(\omega_l t + \alpha t^2)} (\sigma_{23} + \sigma_{14}) + \text{H.c.}$ Here, ω_h and ω_v are the frequencies of the H- and V-polarized cavity modes with annihilation operators a and b , respectively, and $\sigma_{ij} = |i\rangle\langle j|$. The parameters g_h and g_v denote the coupling strengths between the cavity modes and the quantum dot transitions.

The Rabi frequency describing the coupling between the laser pulse and the H-polarized transitions is given by $\Omega_h(t) = \mu E(t)/\hbar$, where μ is the electric dipole moment and the electric field envelope is $E(t) = E_0 \exp\left[-(t - 2.5\tau_p)^2/\tau_p^2\right]$. The full

width at half maximum of the pulse is $\tau_{\text{FWHM}} = 1.177\tau_p$, and α is the linear chirp parameter.

Transforming into a frame rotating at the laser frequency ω_l , the Hamiltonian becomes $H_r = U^\dagger H U + i(\partial U^\dagger / \partial t)U$, with $U = \exp[-i\omega_l t(a^\dagger a + b^\dagger b + \sigma_{33} + \sigma_{44})]$. This yields $H_r = H_0^r + H_{\text{int}}^r$, where $H_0^r = -\frac{\delta_e}{2}\sigma_{11} + \frac{\delta_e}{2}\sigma_{22} + \left(\Delta - \frac{\delta_e}{2}\right)\sigma_{33} + \left(\Delta + \frac{\delta_h}{2}\right)\sigma_{44} + \Delta_{hl} a^\dagger a + \Delta_{vl} b^\dagger b$ and $H_{\text{int}}^r = g_h a^\dagger (\sigma_{14} + \sigma_{23}) + i g_v b^\dagger (\sigma_{24} + \sigma_{31}) + \Omega_h e^{i\alpha t^2} (\sigma_{23} + \sigma_{14}) + \text{H.c.}$ Here, $\Delta = \omega_0 - \omega_l$, $\Delta_{hl} = \omega_h - \omega_l$, $\Delta_{vl} = \omega_v - \omega_l$, and $\Delta_{HV} = \omega_h - \omega_v$.

To investigate single-photon generation, we numerically solve the master equation $d\rho/dt = -i[H_r, \rho] + \mathcal{L}_{\text{cav}}\rho + \mathcal{L}_{\text{QD}}^r\rho + \mathcal{L}_{\text{QD}}^d\rho$, where $\mathcal{L}_{\text{cav}}\rho = (\kappa/2)[\mathcal{L}(a)\rho + \mathcal{L}(b)\rho]$, $\mathcal{L}_{\text{QD}}^r\rho = (\Gamma_{14}/2)\mathcal{L}(\sigma_{14})\rho + (\Gamma_{24}/2)\mathcal{L}(\sigma_{24})\rho + (\Gamma_{13}/2)\mathcal{L}(\sigma_{13})\rho + (\Gamma_{23}/2)\mathcal{L}(\sigma_{23})\rho$, and $\mathcal{L}_{\text{QD}}^d\rho = (\gamma_{33}/2)\mathcal{L}(\sigma_{33})\rho + (\gamma_{44}/2)\mathcal{L}(\sigma_{44})\rho$, with the Lindblad superoperator defined as $\mathcal{L}(o)\rho = 2op\rho^\dagger - o^\dagger o\rho - \rho o^\dagger o$.

3. RESULTS AND DISCUSSIONS

We investigate the single-photon parameters, including indistinguishability, brightness, and the multiphoton emission probability, by numerically solving the master equation together with the quantum regression theorem. In the simulations, we choose typical parameters for the quantum dot and cavity system: $\Gamma_{14} = \Gamma_{24} = \Gamma_{13} = \Gamma_{23} = 1\text{ }\mu\text{eV}$, $\gamma_{33} = \gamma_{44} = 2\text{ }\mu\text{eV}$, $g_e = 0.378$, $g_h = 0.202$, $\mu_B = 0.578\text{ }\mu\text{eV}$, and $B = 5\text{ T}$ [36]. The remaining parameters are chosen as $g_h = g_v = 60\text{ }\mu\text{eV}$ for resonant excitation and $g_h = g_v = 70\text{ }\mu\text{eV}$ for adiabatic excitation, $\alpha = 7\text{ ps}^{-2}$ for adiabatic excitation and $\alpha = 0$ for resonant excitation, and a cavity decay rate of $\kappa = 150\text{ }\mu\text{eV}$.

A. Indistinguishability and Brightness of Single-Photon

The purity of the emitted photon's quantum state is quantified by its single-photon indistinguishability. When the probability of emitting more than one photon is negligible, indistinguishability reflects the first-order (field) coherence of the source, indicating that the spectra of the emitted photon wave packets are mutually identical. However, when the source exhibits a nonzero probability of multiphoton emission, the indistinguishability is no longer determined solely by first-order coherence. In such cases, particularly for pulse-triggered single-photon sources, it also depends critically on the second-order (intensity) coherence, since multiphoton contributions degrade the overall purity of the quantum state. Experimentally, a Mach-Zehnder interferometer can be used to measure the indistinguishability of a single-photon source, triggered with a delay much longer than the lifetime of the excited states [37].

In Figs. 2 and 3, we present the single-photon indistinguishability I and brightness β as functions of the Rabi frequency and pulse duration for resonant excitation ($\alpha = 0$) and adiabatic excitation ($\alpha = 7\text{ ps}^{-2}$), respectively. The mathematical expressions used to compute these quantities are provided in Appendix A. From Figs. 2 (a) and 3 (a), it is evident that adiabatic excitation yields a significantly higher indistinguishability, exceeding 0.98, compared to the value of approximately 0.92 obtained under resonant excitation. This improvement primarily arises from the substantially reduced multiphoton emission probability for adiabatic excitation, as discussed in the next section. Moreover, as expected, the indistinguishability achieved through adiabatic rapid passage is considerably more robust against variations in both the Rabi frequency and the pulse duration, whereas the resonant scheme shows a stronger sensitivity to these parameters.

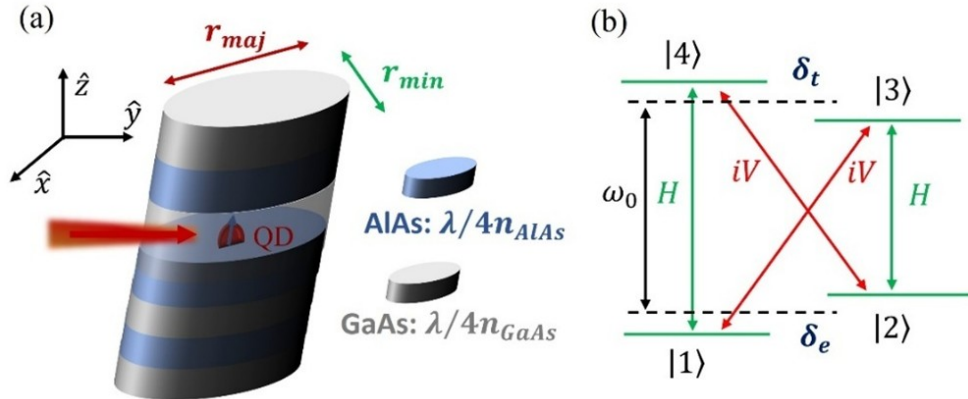


Fig. 1. (a) Illustration of an elliptical pillar microcavity comprising GaAs/AlAs distributed Bragg reflectors with an embedded negatively charged quantum dot (QD). (b) Energy-level diagram and optical transitions of a four-level QD system induced by an externally supplied magnetic field in the Voigt configuration. A description of the different energy levels and optical transitions is provided in the text.

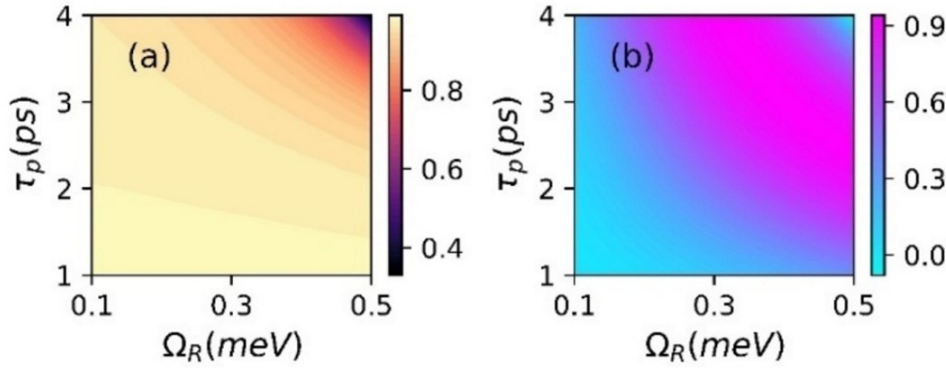


Fig. 2. Evolution of the (a) indistinguishability and (b) brightness as a function of Rabi frequency and pulse duration for resonant excitation with $\Delta_{HV} = 0.6$ meV.

Similarly, the brightness obtained under adiabatic excitation is not only higher but also more robust and stable compared to that achieved with resonant excitation, as evident from Figs. 2 (b) and 3 (b).

Next, in Figs. 4 and 5, we investigate the indistinguishability I and brightness β as functions of Δ_{HV} for resonant and adiabatic excitation, respectively. In both cases, I and β increase with increasing Δ_{HV} . This behavior arises because, for larger Δ_{HV} , the emission from state $|3\rangle$ is preferentially funneled into the V-polarized cavity mode, which is resonant with the $|1\rangle \leftrightarrow |3\rangle$ transition. At the same time, the probability of emission into the H-polarized cavity mode, mediated by the $|2\rangle \leftrightarrow |3\rangle$ and $|1\rangle \leftrightarrow |4\rangle$ transitions, is significantly suppressed. As a result, multiphoton emission events are reduced, leading to enhanced single-photon indistinguishability and brightness.

B. Probability of Multiphoton Emission and Secure Key Rate

Next, we analyze the probabilities of single- and two-photon emission from the quantum-dot source under both resonant and adiabatic excitation, and compare the resulting secure key rate (SKR) with those obtained using quantum dot source (QDS) and PDS sources. Throughout this work, we have neglected the probability of generating three or more photons, as the n -photon generation probability for three-level systems scales as

$(\Gamma \tau_{FWHM})^{2(n-1)}$ [38]. For the chosen parameters, the probability of three-photon generation, p_3 , scales as 10^{-9} , which is negligibly small. The detailed expressions for the multiphoton emission probabilities and the SKR for BB84 and TF-QKD are summarized in Appendix A and B, respectively. From Figs. 6 and 7, it is evident that the single-photon generation probability increases, while the two-photon emission probability simultaneously decreases with increasing Δ_{HV} for both resonant and adiabatic excitation.

Notably, the two-photon emission probability under adiabatic excitation is at least an order of magnitude lower than that achieved with resonant excitation. Consequently, the performance of the quantum-dot source under adiabatic excitation is slightly superior to that under resonant excitation, as illustrated in Figs. 8 and 9. To compare the performance of QDS and PDS sources for BB84 QKD (without decoy and with infinite decoy states) and TF-QKD with infinite decoy states, we plot the SKR per pulse as a function of the source efficiency.

As shown in Fig. 8, the SKR for the PDS source reaches a maximum at an optimal source efficiency; beyond this point, the increasing contribution of multiphoton pulses leads to a rapid degradation of the SKR, eventually driving it to zero. In contrast, for QDS under both adiabatic excitation (AE) and resonant excitation (RE), the SKR increases nearly linearly with source

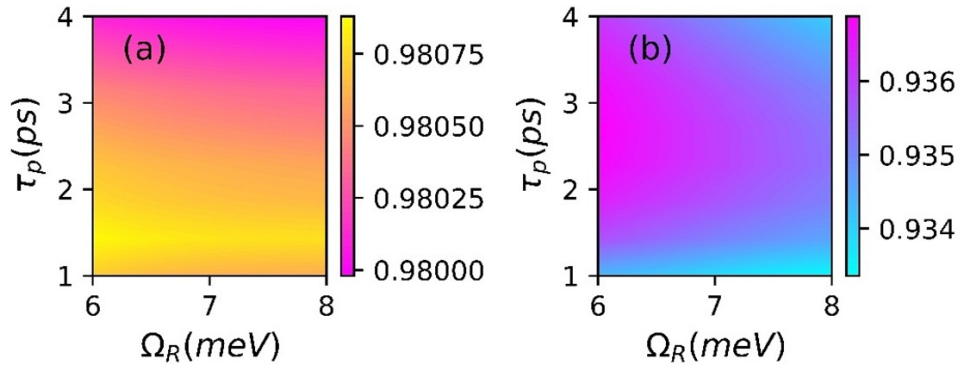


Fig. 3. Evolution of the (a) indistinguishability and (b) brightness as a function of Rabi frequency and pulse duration for adiabatic excitation with $\Delta_{HV} = 0.6$ meV.

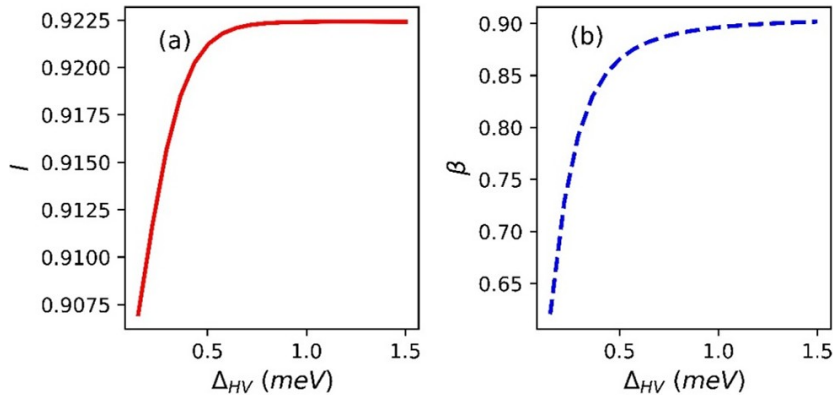


Fig. 4. Evolution of (a) the indistinguishability and (b) the brightness as functions of the frequency separation between the cavity modes, Δ_{HV} , for $\tau = 2.8$ ps and $\Omega_R = 0.4$ meV under resonant excitation.

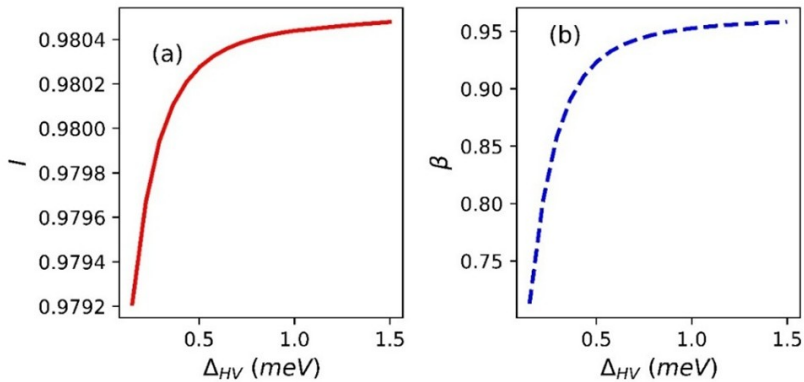


Fig. 5. Evolution of (a) the indistinguishability and (b) the brightness as functions of the frequency separation between the cavity modes, Δ_{HV} , for $\tau = 2.8$ ps and $\Omega_R = 0.4$ meV under adiabatic excitation.

efficiency because the vacuum and single-photon components remain dominant across the entire efficiency range. Notably, the AE-driven QDS achieves a slightly higher SKR than the RE-driven QDS, owing to its reduced multiphoton emission probability.

In Fig. 9, we present the performance of the QDS pumping schemes for collection efficiencies ranging from 1% to 100%, and compare these results with the optimal performance of phase-randomized (PR) PDS at its best choice of μ . As shown in Fig. 9(a), the SKR achieved with QDS is consistently higher, en-

abling secure communication over significantly longer distances. Even with a collection efficiency of only 1%, QDS supports a substantially longer transmission distance than PR-PDS; this advantage increases to at least a threefold improvement when the collection efficiency reaches 100%. Furthermore, Figs. 9(b) and 9(c) show that the SKR obtained with QDS exceeds that of PDS over short and intermediate distances; however, at longer distances, PDS sources eventually marginally outperform quantum-dot sources in both decoy-state BB84 and TF-QKD.

So far, the simulation of the secure key rate for the considered

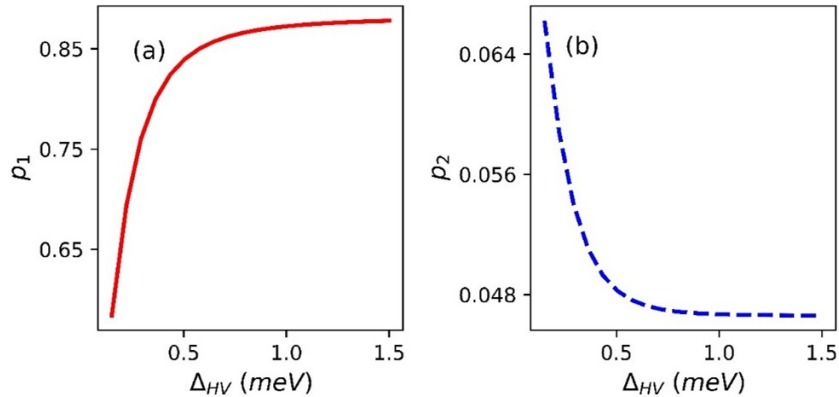


Fig. 6. Evolution of the (a) indistinguishability and (b) brightness as a function of the frequency separation between the cavity modes, Δ_{HV} , for $\tau = 2.8$ ps and $\Omega_R = 0.4$ meV under resonant excitation.

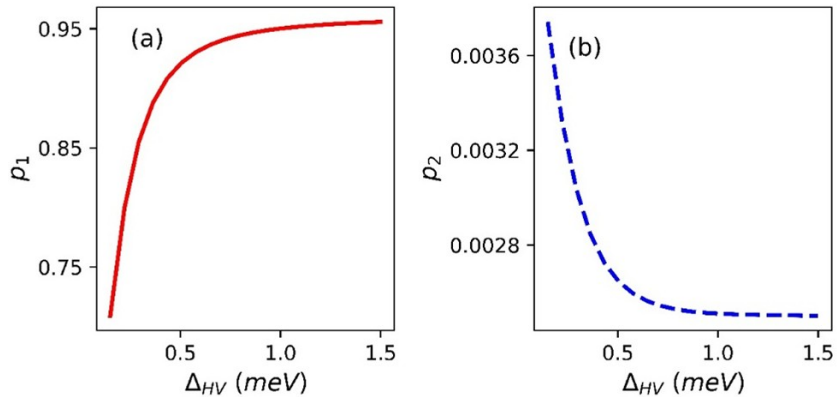


Fig. 7. Evolution of the (a) indistinguishability and (b) brightness as a function of the frequency separation between the cavity modes, Δ_{HV} , for $\tau = 2.8$ ps and $\Omega_R = 0.4$ meV under adiabatic excitation.

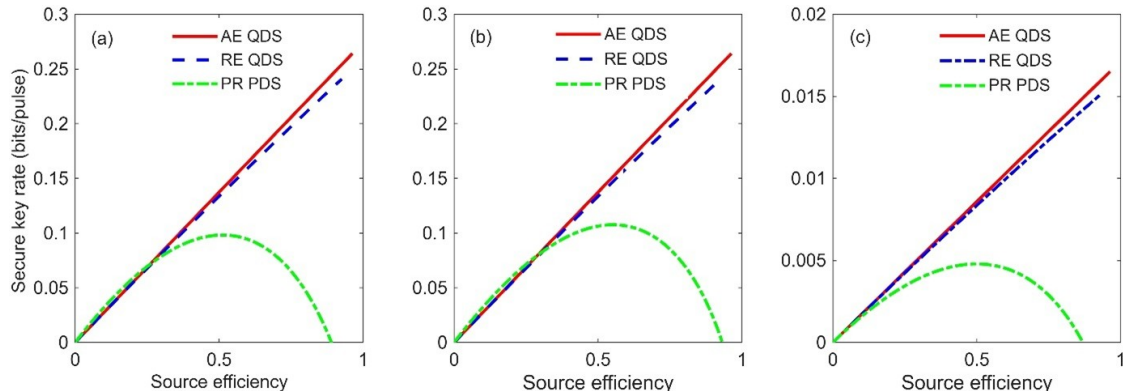


Fig. 8. Evolution of the secure key rate for three QKD schemes as a function of source efficiency for AE QDS (red lines), RE QDS (dashed blue lines), and phase-randomized (PR) PDS (green dashed-dotted). (a) BB84 without decoy states, (b) BB84 with infinite decoy states, (c) twin-field with infinite decoy states. The source efficiency is defined as $1 - e^{-\mu}$ for PDS and $1 - \sum_{n=0}^{\infty} p_n (1 - \eta)^n$ for QDS, where p_n is the n -photon emission probability and η is the QDS collection efficiency. Simulation parameters for all plots are: alignment error rate $e_d = 2\%$, basis reconciliation factor $q = 0.5$, dark count probability $Y_0 = 10^{-9}$, detection efficiency $\eta_d = 100\%$, and error-correcting code inefficiency $f = 1.2$, $d = 1$, $M = 16$, $e_s = 1.275\%$ for TF-QKD. The single- and two-photon emission probabilities are $p_1 = 0.88$ and $p_2 = 4.6 \times 10^{-2}$ under resonant excitation, and $p_1 = 0.96$ and $p_2 = 2.5 \times 10^{-3}$ under adiabatic excitation, respectively, at $\Delta_{HV} = 1.5$ meV.

QKD protocols have assumed ideal detectors with unity efficiency. To assess practical performance of TF-QKD, we investigate the dependence of the secure key rate on detector efficiency for

both PDS and QDS sources. As shown in Figs. 10(a) and 10(b), the secure key rate increases monotonically with detector efficiency, with efficiencies comparable to those of superconducting

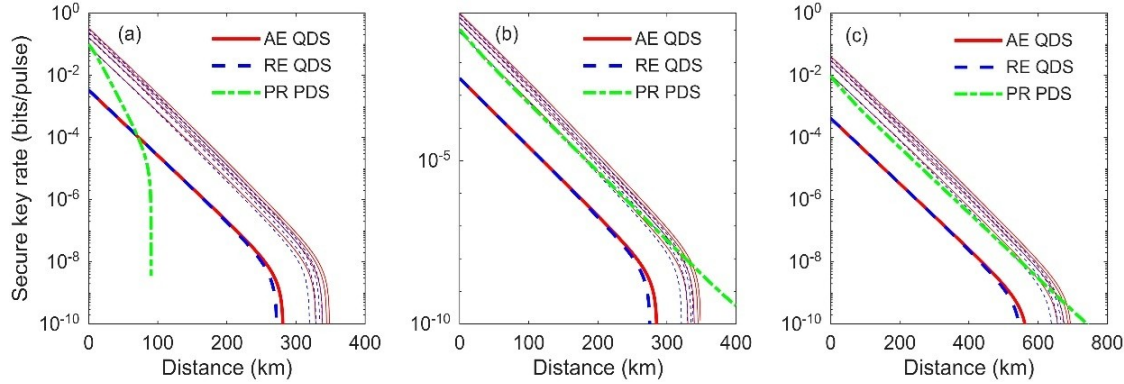


Fig. 9. Evolution of the secure key rate for three QKD schemes as a function of distance for $\alpha = 0.21$ dB/km. (a) BB84 without decoy states with optimal value of $\mu = 0.7 \eta_d \eta_t$, (b) BB84 with infinite decoy states for optimal value of $\mu = 1$, (c) Twin-field with infinite decoy states. The continuum in each plot shows the attainable key rates for AE QDS (red lines) and RE QDS (dashed blue lines) ranging from 1% to 100% collection efficiencies, with intermediate curves showing steps of 20%. The green dashed-dotted line indicates the optimal performance of phase-randomized (PR) PDS. Simulation parameters for TF-QKD are $d = 1$, $M = 16$, $e_s = 1.275\%$, and the optimal value of $\mu = 0.765$. Other parameters are the same as those used in Fig. 8.

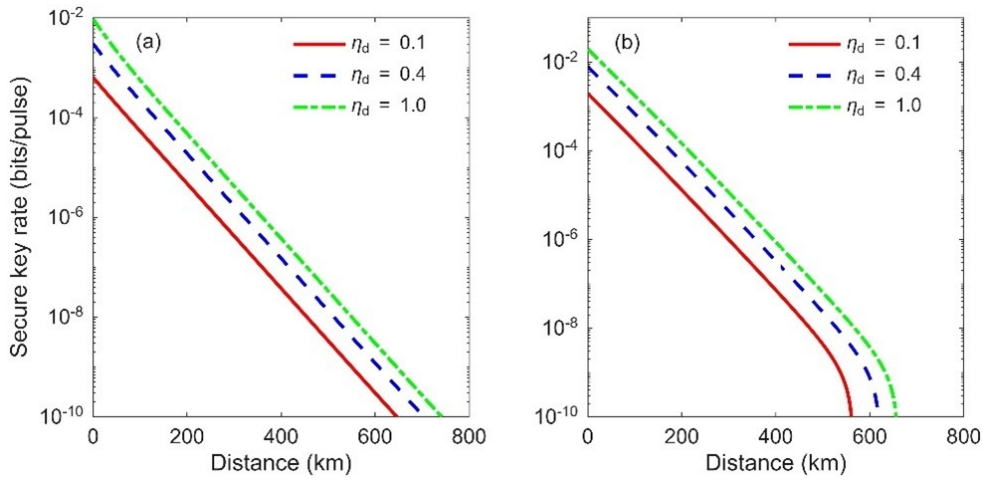


Fig. 10. Evolution of the TF-QKD secure key rate as a function of transmission distance for three different detector efficiencies: (a) Poissonian-distributed coherent sources, and (b) quantum dot sources (QDS) under adiabatic excitation with a collection efficiency of 50%. All other system parameters are identical to those used in Fig. 9.

nanowire single-photon detectors (SNSPDs), typically exceeding 80%, enabling higher key rates and longer transmission distances. Moreover, through similar simulations, we find that the SKR exhibits similar trends for other investigated QKD protocols at different detector efficiencies.

4. CONCLUSION

We have numerically investigated the generation and characterization of single photons from a negatively charged quantum dot embedded in an elliptical pillar microcavity. The spectral nondegeneracy of the cavity modes is shown to significantly suppress the two-photon emission probability, which is a key requirement for quantum key distribution protocols. We further compared two excitation schemes, adiabatic and resonant excitation, and demonstrated that adiabatic excitation provides more robust and stable brightness while achieving a two-photon emission probability that is an order of magnitude lower than that of resonant excitation. Finally, we showed that single photons generated from the quantum dot, under both adiabatic and reso-

nant excitation, clearly outperform Poisson-distributed sources for BB84 QKD without decoy states. Moreover, the proposed quantum-dot single-photon source enables higher secure key rates for both BB84 and original twin-field QKD with infinite decoy states over short and intermediate distances, although at very long distances the secure key rate achievable with PDS becomes slightly higher. These results provide practical insight into the trade-offs between deterministic single-photon sources and conventional Poissonian sources in quantum communication systems.

A. APPENDIX A: INDISTINGUISHABILITY AND BRIGHTNESS OF SINGLE-PHOTON

The indistinguishability of photons emitted into the vertically polarized mode is numerically calculated using [39] as $I = 1 - \frac{\int_0^T dt \int_0^T d\tau [G_{\text{pop}}^2(t, \tau) + g^2(t, \tau) - |g^1(t, \tau)|^2]}{\int_0^T dt \int_0^T d\tau [2G_{\text{pop}}^2(t, \tau) - |\langle b(t+\tau) \rangle \langle b^\dagger(t) \rangle|^2]}$, where $G_{\text{pop}}^2(t, \tau) = \langle b^\dagger b(t) \rangle \langle b^\dagger b(t + \tau) \rangle$, and $g^1(t, \tau)$ and $g^2(t, \tau)$ are the first- and second-order correlation functions, modeled as $g^1(t, \tau) =$

$\langle b^\dagger(t)b(t+\tau) \rangle$ and $g^2(t, \tau) = \langle b^\dagger(t)b^\dagger(t+\tau)b(t+\tau)b(t) \rangle$. The brightness, defined as the emitted cavity photon number per pulse, is $\beta = \kappa \int_0^T \langle b^\dagger b(t) \rangle dt$. The probability of two or more photon emission for a single pulse excitation is given by $\tilde{P}_2 = \frac{\int_0^T dt \int_0^T d\tau g^2(t, \tau)}{\int_0^T dt \int_0^T d\tau \langle b^\dagger(t)b(t) \rangle \langle b^\dagger(t+\tau)b(t+\tau) \rangle}$ [39]. The upper limit of integration T is assumed to be sufficiently long for the quantum dot to relax to its ground state. Moreover, as explained earlier, we assume that the probability of three or more photons is zero, i.e., $\tilde{P}_{\geq 3} = 0$. The single- and two-photon emission probabilities are then $p_1 = \beta - 2\tilde{P}_2$ and $p_2 = \tilde{P}_2$, respectively.

B. APPENDIX B: SECURE KEY RATE FOR BB84 AND TWIN-FIELD QKD PROTOCOLS

The lower bound on the secure key rate for both QDS and PDS single-photon sources is given by $R \geq q[Q_1(1 - H_2(e_1)) - fQ_\mu H_2(E_\mu)]$, where q denotes the basis reconciliation factor ($q = 1/2$ for symmetric basis choice and $q \approx 1$ for efficient BB84 protocols [40]), $Q_\mu = \sum_{n=0}^{\infty} Y_n P_\mu(n)$ is the overall gain, E_μ is the overall QBER, e_1 is the single-photon QBER, f is the error-correction inefficiency, $H_2(\cdot)$ is the binary entropy function, and Y_n is the conditional detection probability (yield) for an n -photon state [18]. The yield of an n -photon pulse is modeled as $Y_n = Y_0 + (1 - Y_0)[1 - (1 - \eta_d \eta_t)^n]$, where Y_0 is the dark count probability, η_d is the detector efficiency, and $\eta_t = 10^{-\alpha L/10}$ is the channel transmission, with α the fiber loss coefficient and L the channel length in km.

Moreover, $P_\mu(n) = \frac{e^{-\mu} \mu^n}{n!}$ represents the photon number distribution for Poisson-distributed sources, including weak coherent pulses and down-conversion sources, where μ is the average photon number [41–44]. The error rate for an n -photon state is $e_n = \frac{e_0 Y_0 + e_d [1 - (1 - \eta_d \eta_t)^n]}{Y_n}$, and the gain for each photon number is $Q_n = Y_n P_\mu(n)$. The overall error rate therefore becomes $E_\mu = \frac{1}{Q_\mu} \sum_{n=0}^{\infty} e_n Q_n$.

A. BB84 QKD Without Decoy States

In the GLLP model for non-decoy BB84, all errors and losses are pessimistically attributed to single-photon components [18]. For $n \geq 2$, one assumes $Y_n = 1$ and $e_n = 0$. Therefore, the single-photon gain and error rate satisfy $Q_1 \geq Q_\mu - \sum_{n \geq 2} P_\mu(n)$ and $e_1 \leq \frac{E_\mu Q_\mu}{Q_1}$. Since multi-photon events are assumed to be fully compromised, the secure communication distance is strongly limited.

B. BB84 QKD With Decoy States

We numerically simulated the BB84 QKD protocol with an infinite number of decoy states, which overcomes the limitation of accurately estimating the single-photon yield and error rate by allowing Alice to vary the mean photon number μ of her transmitted pulses over a continuum of values [21]. Since an eavesdropper cannot distinguish signal from decoy pulses, the channel parameters Y_1 and e_1 can be tightly estimated. In the ideal limit of infinitely many decoy intensities, the single-photon gain satisfies $Q_1 \geq Y_1 P_\mu(1)$, and the single-photon error rate is accurately determined as $e_1 = \frac{e_0 Y_0 + e_d \eta_d \eta_t}{Y_1}$. This greatly enhances both the secret key rate and the maximum feasible communication distance compared to BB84 without decoy states.

C. Twin-Field QKD With Decoy States

In TF-QKD, the detection scheme is closely related to that of phase-encoded decoy-state QKD and consists of single-photon interference followed by threshold single-photon detection. This similarity allows the use of a secure key-rate formula analogous to that of decoy-state QKD, with additional parameters accounting for phase matching and the protocol duty cycle. Specifically, it was shown in a seminal work on TF-QKD that, provided the revelation of the global phase after Charlie's measurement does not increase the eavesdropper's information, the secure key rate of TF-QKD can be written as [26]: $R^{\text{TF}} = \frac{d}{M} [Q_1^{\text{TF}}(1 - H_2(e_1^{\text{TF}})) - f Q_\mu^{\text{TF}} H_2(E_Q^{\text{TF}})]$, where the gain of the n -photon component is $Q_n^{\text{TF}} = Y_n^{\text{TF}} P_\mu(n)$, and the overall gain is $Q_\mu^{\text{TF}} = \sum_{n=0}^{\infty} Y_n^{\text{TF}} P_\mu(n)$. The corresponding error rates are $e_n^{\text{TF}} = \frac{e_0 Y_0 + (e_d + e_s)[1 - (1 - \eta_d \sqrt{\eta_t})^n]}{Y_n^{\text{TF}}}$, $E_Q^{\text{TF}} = \frac{1}{Q_\mu^{\text{TF}}} \sum_{n=0}^{\infty} e_n^{\text{TF}} Q_n^{\text{TF}}$, which have the same functional form as in the infinite-decoy-state QKD analysis. In TF-QKD, unlike BB84, each optical pulse propagates only half of the total distance between Alice and Bob; consequently, the channel transmittance η_t is replaced by $\sqrt{\eta_t}$. Accordingly, the yield of an n -photon component is modeled as $Y_n^{\text{TF}} = Y_0 + (1 - Y_0)[1 - (1 - \eta_d \sqrt{\eta_t})^n]$. The intrinsic error rate $e_s = \frac{1}{2} - \frac{\sin(2\pi/M)}{4\pi/M}$ arises from finite phase slicing, where M denotes the number of phase slices used for phase matching and d is the fraction of protocol rounds allocated to key generation. For finite-decoy-state TF-QKD, modified expressions for the gain and error rates must be employed [45]. To evaluate the secure key rate for a quantum-dot single-photon source (QDS) in both BB84 and TF-QKD, the Poisson photon-number distribution $P_\mu(n)$ is replaced by $P_\eta(n)$. The photon-number probabilities for a QDS are given by $P_\eta(0) = p_0 + p_1(1 - \eta) + p_1(1 - \eta)^2$, $P_\eta(1) = p_1 \eta + p_2[1 - \eta^2 - (1 - \eta)^2]$, $P_\eta(n \geq 2) = 1 - P_\eta(0) - P_\eta(1)$ [31].

ACKNOWLEDGMENT

P.K. acknowledges the grants (SRG/2023/000560) from ANRF (SERB) and NQM, DST, Government of India.

Disclosures

The authors declare no conflicts of interest.

Data availability

The data that support the findings of this study are available upon reasonable request from the authors.

REFERENCES

1. C. H. Bennett and G. Brassard, "Quantum cryptography: public key distribution and coin tossing," *Theor. Comput. Sci.* **560**, 7–11 (2014).
2. C. H. Bennett, F. Bessette, G. Brassard, L. Salvail, and J. A. Smolin, "Experimental quantum cryptography," *J. Cryptol.* **5**, 3–28 (1992).
3. C. H. Bennett, "Quantum cryptography using any two nonorthogonal states," *Phys. Rev. Lett.* **68**, 3121–3124 (1992).
4. C. H. Bennett, G. Brassard, and N. D. Mermin, "Quantum cryptography without Bell's theorem," *Phys. Rev. Lett.* **68**, 557–559 (1992).
5. A. Acín, N. Gisin, and L. Masanes, "From Bell's theorem to secure quantum key distribution," *Phys. Rev. Lett.* **97**, 120405 (2006).
6. J.-G. Ren, P. Xu, H.-L. Yong, et al., "Ground-to-satellite quantum teleportation," *Nature* **549**, 70–73 (2017).
7. M. Zahid, M. T. Mikkelsen, R. Müller, et al., "Quantum key distribution using deterministic single-photon sources over a field-installed fibre link," *npj Quantum Inf.* **10**, 2 (2024).

8. H.-Z. Chen, M.-H. Li, Y.-Z. Wang, et al., "Implementation of carrier-grade quantum communication networks over 10,000 km," *npj Quantum Inf.* **11**, 137 (2025).
9. Y.-A. Chen, Q. Zhang, T.-Y. Chen, et al., "An integrated space-to-ground quantum communication network over 4,600 kilometres," *Nature* **589**, 214–219 (2021).
10. T.-Y. Chen, X. Jiang, S.-B. Tang, et al., "Implementation of a 46-node quantum metropolitan area network," *npj Quantum Inf.* **7**, 134 (2021).
11. B. Baghdasaryan, F. Steinlechner, and S. Fritzsche, "Enhancing the purity of single photons in parametric down-conversion," *Phys. Rev. A* **108**, 023718 (2023).
12. X. You and Y.-M. He, "Developing quantum-dot single-photon sources with excellent performance by coupling asymmetric microcavities," *Phys. Rev. Res.* **7**, L012016 (2025).
13. P. Kumar and A. G. Vedeshwar, "Phonon-assisted control of the single-photon spectral characteristics," *Phys. Rev. A* **96**, 033808 (2017).
14. S. Park, K.M. Azizur-Rahman, D. Shima, et al., "Efficient single-photon emission via quantum-confined charge funneling to quantum dots," *Commun. Mater.* **6**, 286 (2025).
15. S. Kikura, R. Asaoka, M. Koashi, and Y. Tokunaga, "High-purity single-photon generation based on cavity QED," *Phys. Rev. Res.* **7**, 013251 (2025).
16. H.-K. Lo and H. F. Chau, "Unconditional security of quantum key distribution over arbitrarily long distances," *Science* **283**, 2050–2056 (1999).
17. D. Gottesman and H.-K. Lo, "Proof of security of quantum key distribution with two-way classical communications," *IEEE Trans. Inf. Theory* **49**, 457–475 (2003).
18. D. Gottesman, H.-K. Lo, N. Lütkenhaus, and J. Preskill, "Security of quantum key distribution with imperfect devices," *Quantum Inf. Comput.* **4**, 325–360 (2004).
19. N. Gisin, G. Ribordy, W. Tittel, and H. Zbinden, "Quantum cryptography," *Rev. Mod. Phys.* **74**, 145–195 (2002).
20. G. Brassard, N. Lütkenhaus, T. Mor, and B.C. Sanders, "Limitations on practical quantum cryptography," *Phys. Rev. Lett.* **85**, 1330–1333 (2000).
21. H.-K. Lo, X. Ma, and K. Chen, "Decoy state quantum key distribution," *Phys. Rev. Lett.* **94**, 230504 (2005).
22. W.-Y. Hwang, "Quantum key distribution with high loss: Toward global secure communication," *Phys. Rev. Lett.* **91**, 057901 (2003).
23. V. Scarani, H. Bechmann-Pasquinucci, N.J. Cerf, et al., "The security of practical quantum key distribution," *Rev. Mod. Phys.* **81**, 1301–1350 (2009).
24. F. Xu, X. Ma, Q. Zhang, H.-K. Lo, and J.-W. Pan, "Secure quantum key distribution with realistic devices," *Rev. Mod. Phys.* **92**, 025002 (2020).
25. X. Ma, B. Qi, Y. Zhao, and H.-K. Lo, "Practical decoy-state quantum key distribution," *Phys. Rev. A* **72**, 012326 (2005).
26. M. Lucamarini, Z. L. Yuan, J. F. Dynes, and A. J. Shields, "Overcoming the rate–distance limit of quantum key distribution without quantum repeaters," *Nature* **557**, 400–403 (2018).
27. X. Ma, P. Zeng, and H. Zhou, "Phase-matching quantum key distribution," *Phys. Rev. X* **8**, 031043 (2018).
28. Z.-W. Yu, X.-L. Hu, C. Jiang, et al., "Sending-or-not-sending twin-field quantum key distribution in practice," *Sci. Rep.* **9**, 3080 (2019).
29. X.-L. Hu, C. Jiang, Z.-W. Yu, and X.-B. Wang, "Sending-or-not-sending twin-field protocol for quantum key distribution with asymmetric source parameters," *Phys. Rev. A* **100**, 062337 (2019).
30. H.-L. Yin and Z.-B. Chen, "Coherent-state-based twin-field quantum key distribution," *Sci. Rep.* **9**, 14918 (2019).
31. M. Bozzio, M. Vyvlečka, M. Cosacchi, A. Rastelli, and V. Zwiller, "Enhancing quantum cryptography with quantum dot single-photon sources," *npj Quantum Inf.* **8**, 104 (2022).
32. P. Laccotripes, T. Müller, R. M. Stevenson, et al., "Spin–photon entanglement with direct photon emission in the telecom C band," *Nat. Commun.* **15**, 9740 (2024).
33. M. Wasiluk, H. Janowska, A. Musiał, et al., "Probing electron spin dynamics in single telecom InAs(P)/InP quantum dots using the Hanle effect," *Appl. Phys. Lett.* **127**, 204001 (2025).
34. H. Wang, Y.-M. He, T.-H. Chung, et al., "Towards optimal single-photon sources from polarized microcavities," *Nat. Photonics* **13**, 770 (2019).
35. U. M. Gür, M. Mattes, S. Arslanagić, and N. Gregersen, "Elliptical micropillar cavity design for highly efficient polarized emission of single photons," *Appl. Phys. Lett.* **118**, 061101 (2021).
36. A. Majumdar, P. Kaer, M. Bajcsy, et al., "Proposed coupling of an electron spin in a semiconductor quantum dot to a nanoscale optical cavity," *Phys. Rev. Lett.* **111**, 027402 (2013).
37. K. A. Fischer, K. Müller, K. G. Lagoudakis, and J. Vučković, "Dynamical modeling of pulsed two-photon interference," *New J. Phys.* **18**, 113053 (2016).
38. L. Hanschke, K. A. Fischer, S. Appel, et al., "Quantum dot single-photon sources with ultra-low multiphoton probability," *npj Quantum Inf.* **4**, 43 (2018).
39. C. Gustin and S. Hughes, "Pulsed excitation dynamics in quantum-dot–cavity systems: Limits to optimizing the fidelity of on-demand single-photon sources," *Phys. Rev. B* **98**, 045309 (2018).
40. H.-K. Lo, H. F. Chau, and M. Ardehali, "Efficient quantum key distribution scheme and a proof of its unconditional security," *J. Cryptol.* **18**, 133 (2005).
41. H. de Riedmatten, V. Scarani, I. Marcikic, et al., "Two independent photon pairs versus four-photon entangled states in parametric down-conversion," *J. Mod. Opt.* **51**, 1637 (2004).
42. B. Blauensteiner, I. Herbauts, S. Bettelli, A. Poppe, and H. Hübel, "Photon bunching in parametric down-conversion with continuous-wave excitation," *Phys. Rev. A* **79**, 063846 (2009).
43. W. Mauerer, M. Avenhaus, W. Helwig, and C. Silberhorn, "How colors influence numbers: Photon statistics of parametric down-conversion," *Phys. Rev. A* **80**, 053815 (2009).
44. H. Takesue and K. Shimizu, "Effects of multiple pairs on visibility measurements of entangled photons generated by spontaneous parametric processes," *Opt. Commun.* **283**, 276 (2010).
45. Q. Peng, J.-P. Chen, T. Xing, D. Wang, Y. Wang, Y. Liu, and A. Huang, "Practical security of twin-field quantum key distribution with optical phase-locked loop under wavelength-switching attack," *npj Quantum Inf.* **11**, 7 (2025).